ARTICLE

www.the-innovation.org

Rapid, artifact-reduced, image reconstruction for super-resolution structured illumination microscopy

Zhaojun Wang,[1,7] Tianyu Zhao,[1,7] Yanan Cai,[2] Jingxiang Zhang,[1] Huiwen Hao,[3] Yansheng Liang,[1] Shaowei Wang,[1] Yujie Sun,[3] Tongsheng Chen,[4] Piero R. Bianco,[5] Kwangsung Oh,[6] and Ming Lei[1,*]

*Correspondence: ming.lei@mail.xjtu.edu.cn

Received: February 4, 2023; Accepted: April 10, 2023; Published Online: April 13, 2023; https://doi.org/10.1016/j.xinn.2023.100425

GRAPHICAL ABSTRACT

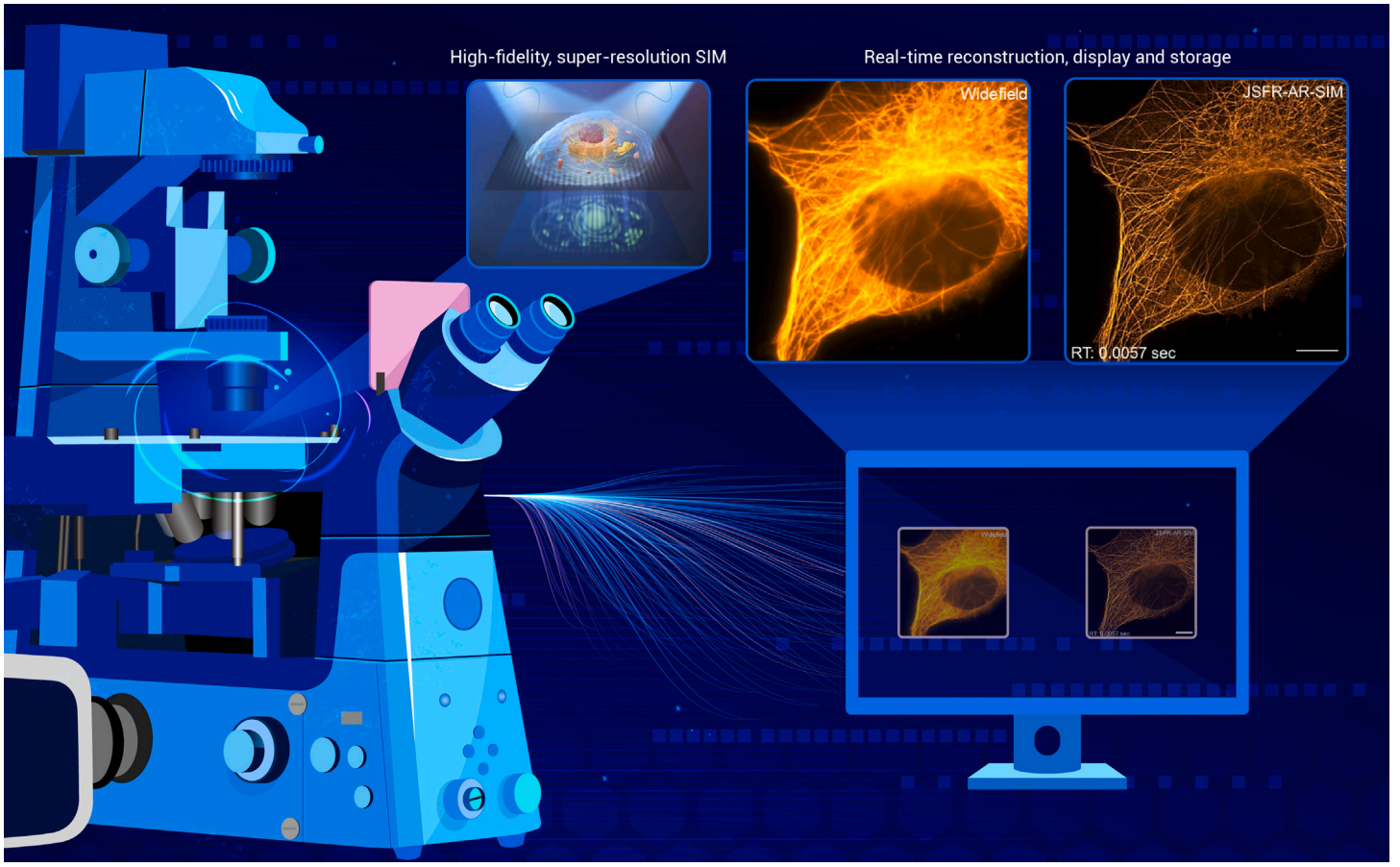

PUBLIC SUMMARY

- Super-resolution structured illumination microscopy is limited by artifacts and postprocessing procedures.
- JSFR-AR-SIM is developed to reconstruct high-quality, super-resolution images with minimal artifacts and increasing efficiency.
- A real-time reconstruction, display, and storage of high-fidelity, super-resolved images of the samples is achieved.

ARTICLE

Rapid, artifact-reduced, image reconstruction for super-resolution structured illumination microscopy

Zhaojun Wang,[1,7] Tianyu Zhao,[1,7] Yanan Cai,[2] Jingxiang Zhang,[1] Huiwen Hao,[3] Yansheng Liang,[1] Shaowei Wang,[1] Yujie Sun,[3] Tongsheng Chen,[4] Piero R. Bianco,[5] Kwangsung Oh,[6] and Ming Lei[1,*]

[1]MOE Key Laboratory for Nonequilibrium Synthesis and Modulation of Condensed Matter, School of Physics, Xi'an Jiaotong University, Xi'an 710049, China

[2]College of Science, Northwest A&F University, Yangling 712100, China

[3]State Key Laboratory of Membrane Biology & Biomedical Pioneer Innovation Center (BIOPIC) & School of Life Sciences, Peking University, Beijing 100871, China

[4]MOE Key Laboratory of Laser Life Science & Guangdong Provincial Key Laboratory of Laser Life Science, College of Biophotonics, South China Normal University, Guangzhou 510631, China

[5]Department of Pharmaceutical Sciences, College of Pharmacy, University of Nebraska Medical Center, Omaha, NE 68198-6025, USA

[6]Department of Computer Science, College of Information Science & Technology, University of Nebraska Omaha, Omaha, NE 68182, USA

[7]These authors contributed equally

*Correspondence: ming.lei@mail.xjtu.edu.cn

Received: February 4, 2023; Accepted: April 10, 2023; Published Online: April 13, 2023; https://doi.org/10.1016/j.xinn.2023.100425

Citation: Wang Z., Zhao T., Cai Y., et al., (2023). Rapid, artifact-reduced, image reconstruction for super-resolution structured illumination microscopy. The Innovation **4(3)**, 100425.

Super-resolution structured illumination microscopy (SR-SIM) is finding increasing application in biomedical research due to its superior ability to visualize subcellular dynamics in living cells. However, during image reconstruction artifacts can be introduced and when coupled with time-consuming postprocessing procedures, limits this technique from becoming a routine imaging tool for biologists. To address these issues, an accelerated, artifact-reduced reconstruction algorithm termed joint space frequency reconstruction-based artifact reduction algorithm (JSFR-AR-SIM) was developed by integrating a high-speed reconstruction framework with a high-fidelity optimization approach designed to suppress the sidelobe artifact. Consequently, JSFR-AR-SIM produces high-quality, super-resolution images with minimal artifacts, and the reconstruction speed is increased. We anticipate this algorithm to facilitate SR-SIM becoming a routine tool in biomedical laboratories.

INTRODUCTION

Far-field super-resolution fluorescence microscopy has drawn considerable interest among biologists as it enables them to visualize the fine details of intracellular structures.[1–4] Consequently, super-resolution structured illumination microscopy (SR-SIM) is finding increasing application in the study of living cells as it enables high-speed imaging while minimizing photodamage.[5–8] Various techniques, devices, and algorithms have been introduced to SR-SIM to further enhance its spatial-temporal resolution and imaging depth, which are in high demand in living-cell imaging.[9–16] Despite these developments over the past several years, SR-SIM has two drawbacks that limit widespread use as an imaging modality.

First, reconstruction artifacts can appear in SR-SIM images thereby decreasing the fidelity of the fine structures, resulting in impaired quantitative analysis.[17] During the past decade, image reconstruction algorithms of SR-SIM have undergone great development. Most of these improvements are based on Wiener-SIM developed by Gustafsson and co-workers,[18,19] which has been widely used in commercial SIM systems and open-source toolboxes for its high resolution and flexibility.[20–22] However, the equivalent optical transfer function (OTF) of the Wiener-SIM protocol exhibits residual peaks and downward kinks at the middle frequency, which is in essence different from the ideal OTF with doubled resolution.[23] After being transformed into real space, the non-smooth distribution of the synthetic OTF for SR-SIM results in sidelobe artifacts in the SR images. To minimize these artifacts, dedicated practical guidelines for SR-SIM have been established for microscopists, including instrument refinement, data acquisition, sample preparation, and parameter settings.[24–26] In addition, reconstruction algorithms have been developed to further suppress the random artifacts induced by low signal levels.[11,27] Also, to address the intrinsic issue of the mismatch between the synthetic OTF of SR-SIM and the ideal OTF with the doubled resolution, Wen et al. engineered the effective point spread function (PSF) into an ideal form, resulting in greatly improved image fidelity.[23] This high-fidelity reconstruction algorithm was termed HiFi-SIM.

The second issue that has plagued SR-SIM since its inception, is an inefficient imaging process resulting from a disjointed workflow and slow, complex, reconstruction algorithms.[28] Currently, in SIM imaging, the image acquisition and reconstruction process are separate, so that the high-resolution image only becomes available after a dedicated postprocessing step in the workflow. If the features that biologists are interested in are too small to resolve in wide-field imaging, they cannot tell whether the area they are imaging contains these fine structures before performing offline reconstruction. Consequently, it can be challenging to locate useful data.

This is no longer an issue as demonstrated in our recent work where we presented the joint spatial frequency reconstruction method (JSFR-SIM).[29] This simplified protocol, executed in the GPU environment, is 80-fold faster than conventional Wiener-SIM and does not compromise spatial resolution or image quality. The significance of this improved reconstruction protocol is that microscopists no longer need to constantly switch between wide-field and SR imaging modes before settling on a satisfactory field of view. Instead, when JSFR-SIM is used, all imaging is performed in SR-SIM mode, with SR images being generated in real time. As this is comparable to using a conventional wide-field microscope, it greatly improves working efficiency. However, JSFR-SIM can still produce SR images with unwanted artifacts. To address this issue, and to produce high-fidelity SR images at high speed, we have combined the JSFR algorithm with HiFi-SIM to form the joint space frequency reconstruction-based artifact reduction algorithm for SR-SIM (JSFR-AR-SIM). In this novel algorithm, the outstanding features of JSFR- and HiFi-SIM are not compromised.

We first demonstrate the performance of JSFR-AR-SIM on images of standard samples of representative structures and biological samples. Next, we evaluated the ability of JSFR-AR-SIM to produce exquisite images of the microtubules in HeLa cells. As anticipated, the algorithm enabled the rapid acquisition of exquisite super-resolution images with no visible artifacts. Consequently, we predict that JSFR-AR-SIM will facilitate the widespread application of SR-SIM in biomedical laboratories, as a real-time, artifact-reduced, super-resolution imaging modality.

RESULTS

Principle of JSFR-AR-SIM

Here, we introduce a high-speed, artifact-reduced, reconstruction method (JSFR-AR-SIM) by combining the merits of HiFi- and JSFR-SIM. That is, we successfully combine the rapid reconstruction speed of our previous JSFR-SIM with the high fidelity of HiFi-SIM. The reconstruction workflow is modified from the previous JSFR-SIM framework in the following ways.

First, considering that the difference between the HiFi- and Wiener-SIM is mainly in the preprocessing procedure and final two-step optimization and that JSFR-SIM is equivalent to the Wiener-SIM protocol, we migrate the initial preprocessing procedures and the final spectrum optimization procedures of HiFi-SIM directly into the JSFR-SIM framework. In other words, the image fidelity of JSFR-SIM is improved by appending a preprocessing step before the reconstruction and replacing the final Wiener deconvolution with a two-step spectrum optimization (see details in supplemental information). The resulting workflow

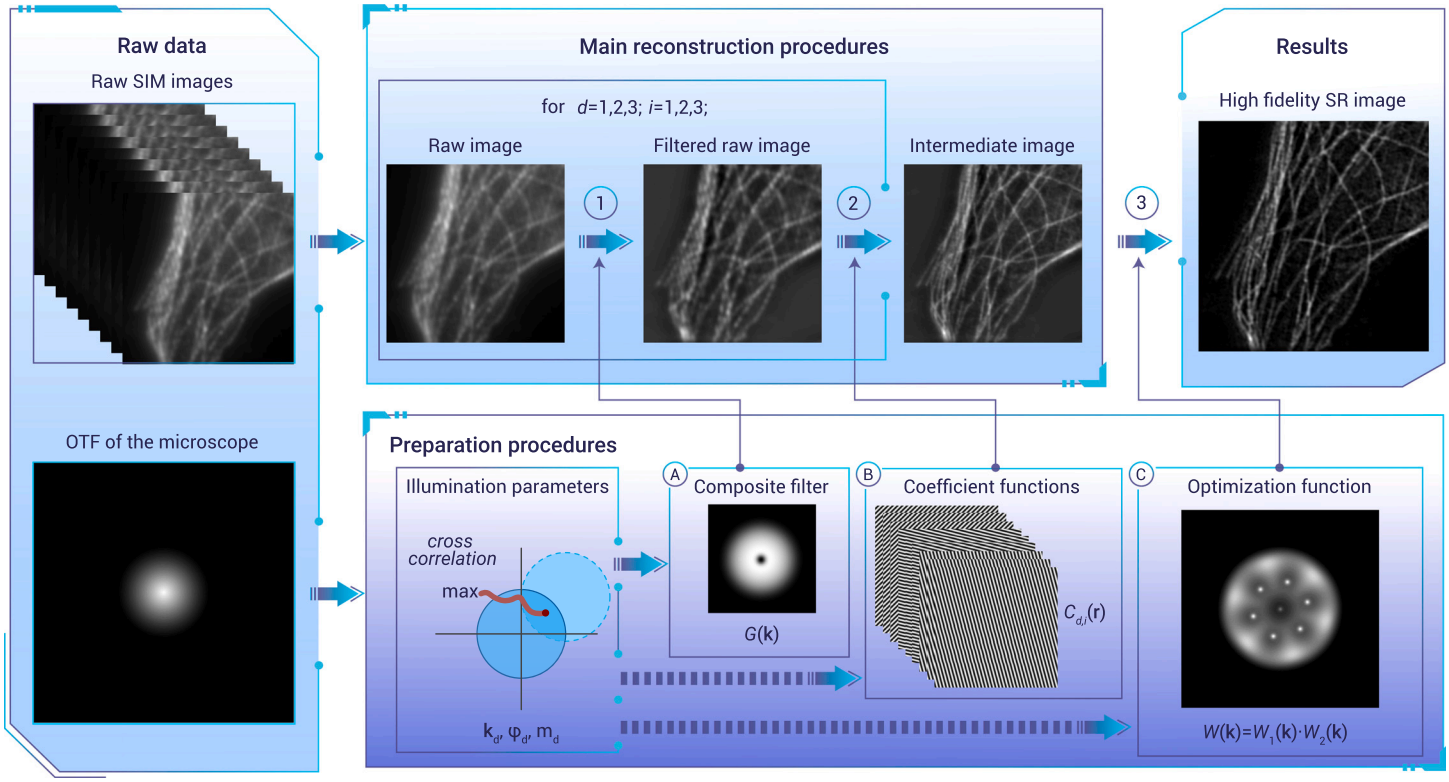

Figure 1. Flowchart of JSFR-AR-SIM The workflow of JSFR-AR-SIM is divided into three main reconstruction procedures and one preparation procedure. In the preparation step, the parameters of the illumination field are obtained by estimation methods, with which the coefficient functions and the optimization functions are calculated for later reconstruction. The main reconstruction is composed of the following three steps: ① First, each raw image is filtered by the composite filter in Equation 2. ② Afterward, an intermediate image is obtained by multiplying the filtered raw images with the corresponding coefficient functions and summing the results up. ③ Eventually, the final image is reconstructed by transforming the product of the spectrum of the intermediate image and the optimization function.

releases the computing burden of HiFi-SIM to some extent because some of the basic procedures in the original algorithm, including the Fourier transform; band separation, shifting, and superposition are simplified to point multiplication and summation in real space. However, the bulk of the computing time required for the preprocessing step and the spectrum optimization remains unchanged (Figure S1).

Secondly, deconvolution in the preprocessing step is an important way to increase the intensity of the high-frequency component, which can reduce the out-of-focus signal-related artifacts and enhancing detection of reconstruction parameters. It is especially important in low-fluorescence signal samples.[30] However, as this has a heavy computing burden (Figure S1), it is crucial to find an equivalent, alternative method to reduce the computation of the preprocessing. Although the iteration number for the RL algorithm used in the HiFi-SIM in the preprocessing postprocessing is limited to 5, it spends much more time than non-iterative deconvolution methods.

As a maximal likelihood estimation of the sample,[16,31–33] RL deconvolution generally reveals a larger expansion in the recovered spectrum than the conventional Wiener deconvolution, as shown in Figures S2E and S2F. However, both HiFi- and JSFR-SIM employed the OTF compensation and attenuation to enhance the spatial resolution and suppress the background fluorescence. This is equivalent to applying a bandpass filter $a(\mathbf{k})\tilde{H}^*(\mathbf{k})$ on all the preprocessed raw images.[29] As such, the extra spectrum information gained by RL deconvolution will be suppressed by the bandpass filter, for which the RL deconvolution does not provide any extra spectrum information of the sample than a Wiener-type filter, as illustrated by Figure S2. Therefore, it makes sense to replace the RL deconvolution in the preprocessing procedure[16,33] with a Wiener-type filter to accelerate the reconstruction speed.

$$D'_{d,j}(\mathbf{r}) = \mathcal{F}^{-1}\left\{\tilde{D}_{d,j}(\mathbf{k}) \cdot \frac{\tilde{H}^*(\mathbf{k})}{|\tilde{H}(\mathbf{k})|^2 + {w_p}^2}\right\} \quad \text{(Equation 1)}$$

Table 1. The JSFR-AR-SIM provides a significantly improved reconstruction speed

Input image size	Output image size	Acquisition time (ms)[a]	Execution time of JSFR-AR-SIM (ms)		Execution time of HiFi-SIM (ms)	
			CPU[b]	GPU[c]	CPU	GPU
2,048 × 2,048	4,096 × 4,096	95.0	5,940.1 ± 776.1 (9.9)[d]	88.7 ± 12.3 (13.7)	58,806.2 ± 1,290.8	1,205.6 ± 13.5
1,024 × 1,024	2,048 × 2,048	45.0	1,340.9 ± 70.8 (10.2)[d]	21.5 ± 6.1 (16.4)	13,720.8 ± 616.0	352.2 ± 6.3
512 × 512	1,024 × 1,024	22.5	274.9 ± 7.3 (12.4)	5.7 ± 4.5 (17.3)	3,412.6 ± 186.6	98.5 ± 3.7
256 × 256	512 × 512	11.3	68.1 ± 1.7 (12.7)	3.1 ± 0.1 (10.0)	866.2 ± 14.3	31.1 ± 0.6

[a]The maximal acquisition time to achieve the frame rate under the corresponding frame size, which adopts the theoretical maximum of the sCMOS camera as described in the materials and methods. As each SR image requires nine raw frames, the acquisition time is calculated by multiplying the raw acquisition time by nine.
[b]The execution time with indicated image dimensions was evaluated using CPU processing as described in the materials and methods. Before reconstruction, the raw images are up-sampled by a factor of 2 to improve the sampling frequency. The values shown are from 2,000 separate processing events of each image, with the times averaged.
[c]The comparison of the reconstruction speed was done using MATLAB (R2022a, The MathWorks). The reconstruction codes for HiFi-SIM and JSFR-AR-SIM (both CPU and the GPU versions) were executed on a personal computer (Intel Core i7-9700K@3.6GHz, DRR4 3200MHz 32GB, NVIDIA GeForce RTX 3080ti 12GB, Samsung 860 EVO 500GB SSD) running Windows 10.
[d]The values in parentheses are the fold increase in processing speed of the JSFR-AR-SIM algorithm relative to HiFi-SIM in the same environment.

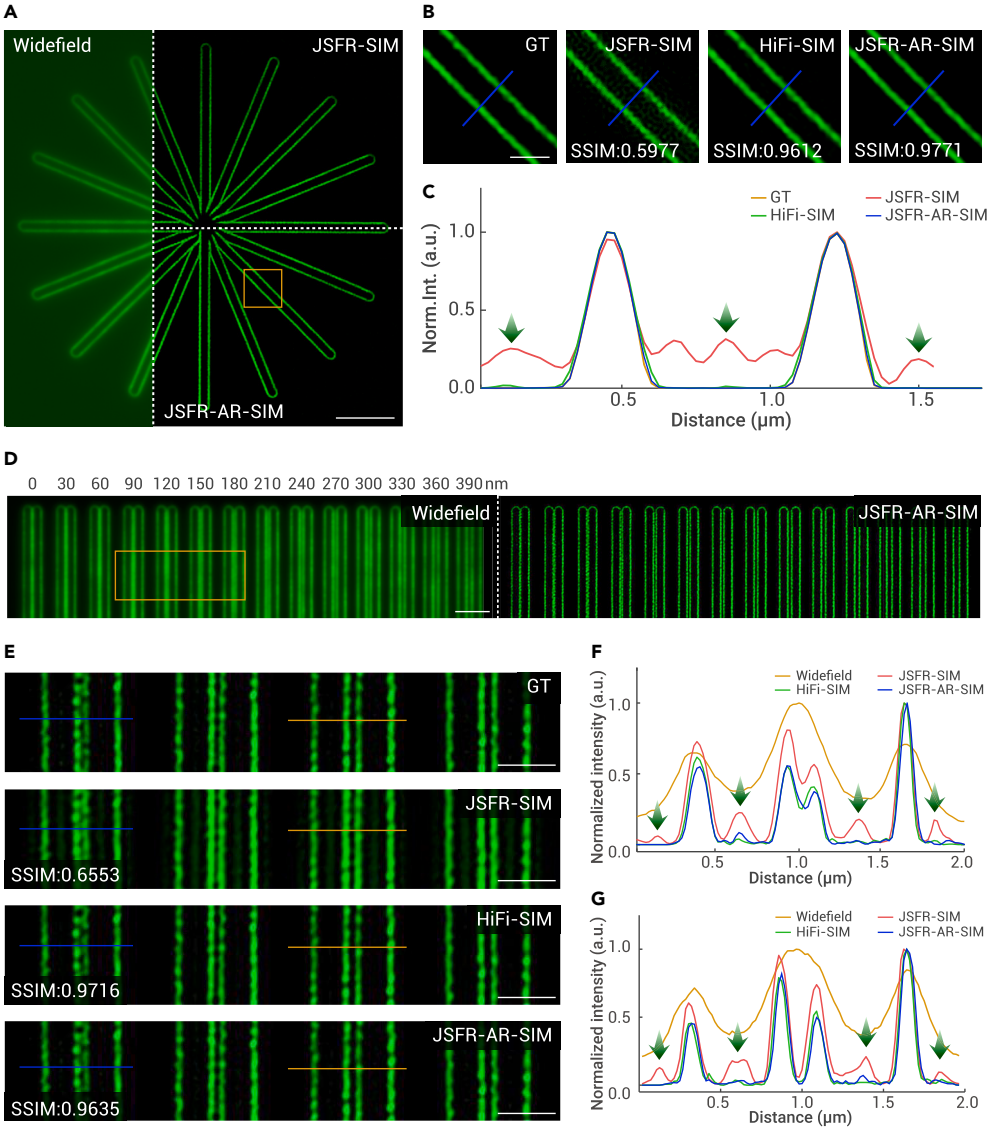

Figure 2. Analysis of Argo-SIM slide images demonstrates the high fidelity of JSFR-AR-SIM (A) Wide-field image of the central part of the star pattern in Argo-SIM slide, and the corresponding SR images recovered with JSFR- and JSFR-AR-SIM ($FWHM_{Apo}$ = 1.1, w_1 = 0.6, w_2 = 1). (B) Close-up view of the yellow box region in the SR images in (A). The ground truth (GT) image was obtained by Wiener-SIM reconstruction of raw data acquired with a 200 ms exposure. (C) Intensity profiles along the blue line in (B). Green arrows, artifacts introduced by image reconstruction. (D) Wide-field and SR images of the resolution test target. The numbers above each line set indicate the distance between two middle lines. (E) Zoomed-in images corresponding to the yellow box in (D). SSIM, structural similarity index measure. (F and G) Intensity profiles corresponding to the blue and yellow lines in (E). Green arrows indicate artifacts introduced by JSFR-SIM reconstruction. Scale bars, 2 μm (A), 500 nm (B), μm (D), and 1 μm (E).

where $\tilde{D}_{d,i}(\mathbf{k})$ denotes the spectrum of the acquired raw images, $\tilde{H}(\mathbf{k})$ indicates the OTF of the microscope, and w_p is the empirical parameter for Wiener deconvolution in the preprocessing procedure. As demonstrated by experimental datasets, no significant change is found in image quality after replacing the RL deconvolution in HiFi-SIM with a Wiener-type filter (Figure S3).

Furthermore, the Wiener-type filter is easily combined with the above band-pass filter $a(\mathbf{k})\tilde{H}^*(\mathbf{k})$, becoming a composite filter

$$\tilde{G}(\mathbf{k}) = \frac{\tilde{H}^*(\mathbf{k})}{|\tilde{H}(\mathbf{k})|^2 + w_p^2} \cdot a(\mathbf{k})\tilde{H}^*(\mathbf{k}) \quad \text{(Equation 2)}$$

where $a(\mathbf{k})$ is the empirical function to attenuate the periodic honeycomb artifacts caused by strong background (see details in supplemental information). In other words, the time-consuming preprocessing procedure in HiFi-SIM is optimized into a single image filter and combined into the initial filtering process in JSFR-SIM. It is worth noting that the composite filter is relevant only to the OTF of the system and the empirical attenuation function, which is static for all successive reconstructions. As such, the computing time of the composite filter can also be decreased by moving it into the preparation procedure. Then, the extra computing burden brought by the RL deconvolution can be eliminated.

In addition, the two optimization functions $\tilde{W}_1(\mathbf{k})$ and $\tilde{W}_2(\mathbf{k})$ in HiFi-SIM do not vary with the sample distribution, and can therefore be combined into a single optimization function $\tilde{W}(\mathbf{k})$ as

$$\tilde{W}(\mathbf{k}) = \tilde{W}_1(\mathbf{k}) \cdot \tilde{W}_2(\mathbf{k}) \quad \text{(Equation 3)}$$

The final super-resolution image is recovered by completing the spectrum optimization (see details in supplemental information).

$$I_{\mathrm{JSFR-AR-SIM}}(\mathbf{r}) = \mathcal{F}^{-1}\left\{\mathcal{F}\left[\sum_{d=1}^{3}\sum_{i=1}^{3} I'^{\,intermediate}_{d,i}(\mathbf{r})\right] \cdot \tilde{W}(\mathbf{k})\right\} \quad \text{(Equation 4)}$$

By pre-computing this combined optimization function in the preparation procedure and reusing it for successive reconstructions, the computing time of the optimization functions could be further saved for continuous image reconstructions.

As a result, the modified protocol can be summarized in the following steps (Figure 1). As a preparation procedure, the parameters of the illumination field are estimated in advance for later use. This includes the wave vectors, initial phases, and modulation depth. Simultaneously, the coefficient functions $c_{d,i}(\mathbf{r})$, the composite filter $\tilde{G}(\mathbf{k})$, and the combined optimization function $\tilde{W}(\mathbf{k})$ for artifact-reduced reconstruction are also pre-computed (see supplemental information). The main reconstruction consists of three steps. First, the raw images are filtered by the composite filter in Equation 2. Second, an intermediate SR image is obtained by superimposing the dot products of the filtered raw images and the pre-calculated coefficient functions. Finally, the artifact-reduced SR image is recovered by multiplying the frequency spectrum of the intermediate SR image with the combined optimization function $\tilde{W}(\mathbf{k})$ and transferring the optimized spectrum back to real space.

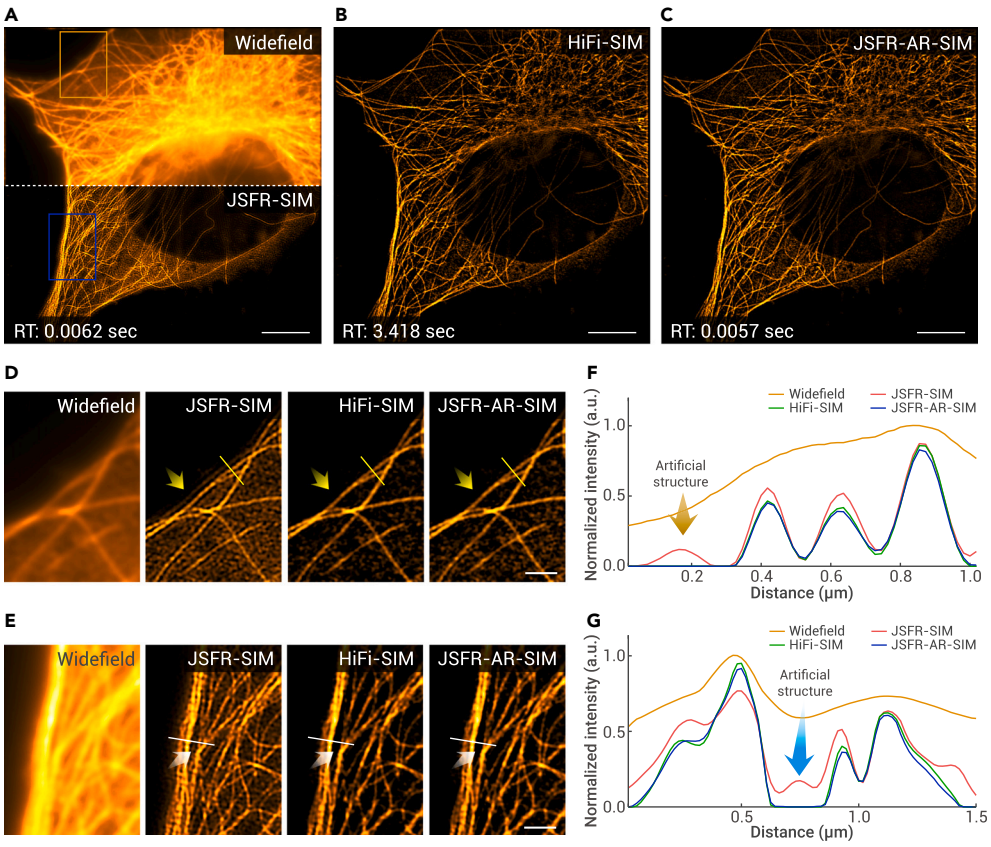

Figure 3. JSFR-AR-SIM enables high-speed, artifact-reduced SR imaging Microtubules were stained with Cy3B and imaged as described in the materials and methods. (A) Pseudo-wide-field image and SR-SIM images reconstructed with JSFR-SIM. (B and C) Artifact-reduced images reconstructed with HiFi- and JSFR-AR-SIM, respectively ($FWHM_{Apo}$ = 1, w_1 = 0.9, w_2 = 0.7). RT, reconstruction time for each SR image. (D and E) Close-up views of the wide-field, JSFR-SIM, HiFi-SIM, and JSFR-AR-SIM images corresponding to the yellow and blue boxes in (A), respectively. Yellow arrows in (D), artificial filament produced by JSFR-SIM. White arrows in (E), the sidelobe of the microtubule recovered by JSFR-SIM. (F and G) Intensity profiles of the yellow and white lines in (D) and (E), respectively. Arrows are artifacts introduced during image reconstruction. Scale bars, 5 μm (A–C) and 1 μm (D and E).

JSFR-AR-SIM accelerates the artifact-reduced reconstruction with a significantly simplified workflow

To demonstrate speed improvement, we evaluated the execution time of JSFR-AR-SIM as a function of image size and compared it with HiFi-SIM (Table 1). In this test, the HiFi-SIM algorithm was rearranged to provide a fair comparison, that is, the preparation procedures such as parameter estimation and the calculation of optimization functions are excluded in the measurement of computing time. Even so, the HiFi-SIM algorithm requires much heavier computing burden than JSFR-AR-SIM (10-fold or more), as demonstrated by the semi-quantitative analysis in Figure S1.

As expected, for each image size in the CPU environment, JSFR-AR-SIM recovers an SR image 10.2- to 12.7-fold faster than HiFi-SIM (Table 1). Furthermore, when executed in the GPU environment, JSFR-AR-SIM gains a 62-fold increase in processing speed for the reconstruction of a 1,024 × 1,024 image, while the HiFi-SIM method achieves only a 39-fold increase. Consequently, JSFR-AR-SIM yields a 600-fold increase over HiFi-SIM in reconstruction speed. Critically, JSFR-AR-SIM reconstructs SR images 2- to 4-fold more rapidly than it takes to acquire them (compare acquisition vs. execution time columns; Table 1). In contrast, the reconstruction speed of the rearranged HiFi-SIM is 2.8- to 7.8-fold slower than the acquisition speed, even when GPU acceleration is used in optimizing the Lucy-Richardson deconvolution and image reconstruction process. Therefore, the significant enhancement in image formation (acquisition plus reconstruction) by JSFR-AR-SIM is much more suitable for real-time SR imaging than HiFi-SIM.

JSFR-AR-SIM produces artifact-reduced SR images of test objects

To validate the artifact reduction capabilities of JSFR-AR-SIM in image reconstruction, we imaged the star and the resolution test target patterns in an Argo-SIM slide (Figures 2 and S4). As the dimension of the parallel line structures is close to the distance of the PSF's sidelobes, the sidelobes of the parallel line structures recovered with JSFR-SIM get incorporated inside parallel lines and, at the periphery, become obvious artificial features (Figures 2A and 2B). These artifacts are visible in the line profiles (Figure 2C, indicated by green arrows). In contrast, both HiFi- and JSFR-AR-SIM suppress these artifacts, yielding clean parallel lines (Figure 2B). This is easily visualized in the intensity profiles, which are almost identical to the ground truth line profile (Figure 2C).

Similarly, the sidelobes of line structures in Figures 2D and 2E are also superimposed as artifacts near the real structures. In the results of JSFR-AR-SIM and HiFi-SIM, no artificial structures are detected (Figures 2F and 2G). By treating the Wiener-SIM result of raw data acquired with long exposure (200 ms) as the ground truth, we quantitatively measure the structural similarity index measure of JSFR-SIM, HiFi-SIM, and JSFR-AR-SIM to be 65.53%, 97.16%, and 96.35% (Figure 2E). This is almost a 50% improvement in the fidelity of JSFR-AR- over JSFR-SIM. Therefore, the speed increase of JSFR-AR-SIM does not come at the expense of the image quality, fidelity, or spatial resolution.

In addition, by comparing the results with different deconvolution parameters in preprocessing procedures (HiFi-SIM: RL iteration number ranges from 1 to 125; JSFR-AR-SIM: Wiener parameter ranges from 0.001 to 0.125), we found that JSFR-AR-SIM is even less sensitive to the deconvolution parameter in the preprocessing procedure than HiFi-SIM (Figure S3). Therefore, JSFR-AR-SIM perfectly inherits the insensitivity to the reconstruction parameters of HiFi-SIM, which therefore avoid frequently adjusting the reconstruction parameter in daily use. To further assess the fidelity of the JSFR-AR-SIM, synthetic and open-access experimental datasets were used (Figures S7–S9). As anticipated, the JSFR-AR-SIM algorithm performs as well as HiFi-SIM. Also, JSFR-AR-SIM has been extended to reconstruct single-layer 3D-SIM datasets (supplemental information), and similar conclusions were achieved (Figures S9 and S10). All these results demonstrate that JSFR-AR-SIM produces SR images with better quality than the widely used Wiener-SIM and the previous JSFR-SIM.

JSFR-AR-SIM produces artifact-reduced SR images of the microtubules in HeLa cells

To demonstrate the ability of JSFR-AR-SIM to rapidly produce super-resolution images, we imaged the microtubules in HeLa cells. In the wide-field image, the extensive network comprising the cytoskeleton is visible but clear visualization is masked by the high background (Figure 3A). This is particularly evident in the very bright region immediately adjacent to the cell nucleus. As expected, each of the reconstruction approaches produces stunning, super-resolution images where the cytoskeleton is clearly visualized (Figure 3A, lower half of the panel; Figures 3B and 3C). To highlight the speed advantage of JSFR-AR-over Hi-SIM (Table 1), we calculated the time required to produce each SR image. The results show that JSFR-AR-SIM is faster (0.0057 vs. 3.418 s).

In addition, the workflow to obtaining an SR image for the two algorithms is drastically different. HiFi-SIM adopts the disjointed workflow where imaging is done first in wide-field mode to locate a field-of-view (Figure 3A, top), followed by switching to SR-SIM mode to acquire the raw images and waiting 3.418 s

to observe the image (Figure 3B). In contrast, for JSFR-AR-SIM, the simplified imaging workflow is done only in SR mode, with a reconstructed image being visualized every 50–100 ms (Figure 3C).[29]

In all SR images, the background fluorescence was well suppressed with OTF attenuation,[29] and the honeycomb artifacts[29,34] induced by strong background in conventional SR-SIM (not presented here) were also eliminated. To demonstrate the ability of algorithms to discern true filaments from artificial ones, we compared two regions of the cytoskeleton image (Figure 3A, yellow and blue boxes).

In the first, the WF image shows an area of high background adjacent to the microtubule at the edge of the cell. Reconstruction by JSFR-SIM introduces a sidelobe artifact parallel to the real structure with an intensity of 20%–30% of the real microtubules (yellow arrows, Figure 3D). In contrast in the HiFi- and JSFR-AR-SIM images, these artifacts are barely detectable (Figure 3F). Similarly, in the second region, JSFR-SIM introduces an artifactual filament positioned between two real filaments (Figure 3E, cyan arrows). This artifact is not present in the high-fidelity images (Figure 3G).

DISCUSSION

Previously, we developed a high-speed framework for SR-SIM, by replacing most of the calculations of the conventional reconstruction with time-saving multiplications and summations in the spatial domain and then executed this novel algorithm in the GPU environment.[29] With this framework, the reconstruction speed of SR-SIM was dramatically increased. However, JSFR-SIM suffered from the sidelobe artifacts originating from the intrinsic imperfection of the synthetic OTF. In this paper, we present a rapid, artifact-reduced reconstruction algorithm for SR-SIM, termed JSFR-AR-SIM. This method greatly simplifies the workflow of the HiFi-SIM by finding an alternative to the time-consuming preprocessing procedure and extending the JSFR concept to high-fidelity image reconstruction. Owing to avoiding iterative deconvolution, the spatial reconstruction algorithm, and GPU acceleration, we can recover an artifact-reduced SR image faster than using HiFi-SIM. Importantly, the image fidelity of the JSFR-AR-SIM is verified to be the same as that of HiFi-SIM, with both being significantly superior to conventional Wiener-SIM. Furthermore, by merging the JSFR-AR-SIM method with the previous real-time observation pipeline,[29] we can easily achieve real-time reconstruction, display, and storage of high-fidelity, super-resolved images of the samples (Figure S11; Video S1). We anticipate that the JSFR-AR-SIM will provide a simple and powerful tool for real-time, accurate super-resolution imaging and analysis of living cells.

As a universal improvement for SR-SIM, this method can be easily extended to other SR-SIM techniques to increase both reconstruction speed and image fidelity.[12,35] Although millisecond-level super-resolution image reconstruction is achieved in the current system, the step of parameter estimation is placed in the preparation procedure and is not counted. It would be suitable for combining with better parameter estimation algorithms to improve the accuracy of reconstructed images. Qian et al.[36] have developed a structured illumination microscopy based on principal-component analysis, which is a novel parameter estimation algorithm with iteration-free reconstruction, robustness to noise, and limited computational complexity. It is possible that combination of the two algorithms might greatly improve the image fidelity, especially in low signal-to-noise ratios. Recently, deep learning algorithms have made significant progress in SIM.[37] It is also possible to combine our algorithm and deep learning methods and improve the imaging speed and quality. In addition to accelerating the image reconstruction speed, JSFR-AR-SIM could also be incorporated into other SIM modalities such as four-frame SR-SIM.[38–40] By reducing the number of frames required to produce an SR image from nine to four, a further increase in overall imaging speed is anticipated. Furthermore, the attributes of JSFR-AR-SIM also provides the potential for SR-SIM to be combined with other imaging modalities such as fluorescence resonance energy transfer microscopy, where real-time feedback combined with high fidelity are required.[41,42]

MATERIALS AND METHODS

Three kinds of samples are used in the experiment. Fluorescent, 40-nm diameter beads, and the commercial Argo-SIM slide were employed as standard specimens to evaluate the performance of JSFR-AR-SIM. The carboxylate-modified fluorophores (yellow-green fluorescent 505/515, F8795, Thermo Fisher Scientific) were first diluted 200 times and dispensed onto the coverslip. The suspension on the coverslip was dried in air for 3 h, and then covered by a drop (3 μL) of Prolong Gold reagent (no. P36934, Thermo Fisher Scientific). The refractive index of Prolong Gold is 1.526, which is close to the refractive index of the mounting medium (1.515) for the oil immersion objective lens, minimizing the spherical aberration caused by refractive index mismatch.

HeLa cells for immunostaining were purchased from American Type Culture Collection. Cells were cultured with high-glucose DMEM with 10% FBS, 1% 100 mM sodium pyruvate solution (Sigma-Aldrich, S8636, and grown under standard cell culture conditions (5% CO_2, humidified atmosphere at 37°C). Before fixation, cells were plated on DMEM/Ham's F-12 pre-incubated glass coverslips for 24 h. The immunostaining process for microtubules consisted of following several steps. First, cells were fixed for 10 min with 3% paraformaldehyde and 0.1% glutaraldehyde in PBS, washed with PBS, and reduced for 5 min with 0.1% sodium borohydride in PBS to minimize the background fluorescence. Then, they were washed with PBS, blocked for 30 min with 3% bovine serum albumin and 0.25% (v/v) Triton X-100 in PBS (blocking buffer 1), stained for 45 min with primary antibody to tubulin (rat anti-tubulin) diluted in blocking buffer 1 to a concentration of 10 mg/mL, and washed with PBS. After being incubated for 45 min with secondary antibodies at a concentration of ~2.5 mg/mL in blocking buffer 1, they were washed with PBS again. Finally, the cells were fixed after labeling for 10 min with 3% paraformaldehyde and 0.1% glutaraldehyde in PBS, and washed with PBS.

REFERENCES

1. Sigal, Y.M., Zhou, R., and Zhuang, X. (2018). Visualizing and discovering cellular structures with super-resolution microscopy. Science ***361***, 880–887.
2. Gao, R., Asano, S.M., Upadhyayula, S., et al. (2019). Cortical column and whole-brain imaging with molecular contrast and nanoscale resolution. Science ***363***, eaau8302.
3. Gwosch, K.C., Pape, J.K., Balzarotti, F., et al. (2020). MINFLUX nanoscopy delivers 3D multicolor nanometer resolution in cells. Nat. Methods ***17***, 217–224.
4. Yu, Z., Li, H., Zhong, T., et al. (2022). Wavefront shaping: a versatile tool to conquer multiple scattering in multidisciplinary fields. Innovation ***3***, 100292–100637.
5. Li, D., Shao, L., Chen, B.-C., et al. (2015). Extended-resolution structured illumination imaging of endocytic and cytoskeletal dynamics. Science ***349***, aab3500.
6. Chen, Q., Shao, X., Tian, Z., et al. (2019). Nanoscale monitoring of mitochondria and lysosome interactions for drug screening and discovery. Nano Res. ***12***, 1009–1015.
7. Qin, J., Guo, Y., Xue, B., et al. (2020). ER-mitochondria contacts promote mtDNA nucleoids active transportation via mitochondrial dynamic tubulation. Nat. Commun. ***11***, 4471:1–12.
8. Segawa, M., Wolf, D.M., Hultgren, N.W., et al. (2020). Quantification of cristae architecture reveals time-dependent characteristics of individual mitochondria. Life Sci. Alliance ***3***, e201900620.
9. Song, L., Lu-Walther, H.-W., Förster, R., et al. (2016). Fast structured illumination microscopy using rolling shutter cameras. Meas. Sci. Technol. ***27***, 055401.
10. Wu, Y., and Shroff, H. (2018). Faster, sharper, and deeper: structured illumination microscopy for biological imaging. Nat. Methods ***15***, 1011–1019.
11. Huang, X., Fan, J., Li, L., et al. (2018). Fast, long-term, super-resolution imaging with Hessian structured illumination microscopy. Nat. Biotechnol. ***36***, 451–459.
12. Guo, Y., Li, D., Zhang, S., et al. (2018). Visualizing intracellular organelle and cytoskeletal interactions at nanoscale resolution on millisecond timescales. Cell ***175***, 1430–1442.e17.
13. Žurauskas, M., Dobbie, I.M., Parton, R.M., et al. (2019). IsoSense: frequency enhanced sensorless adaptive optics through structured illumination. Optica ***6***, 370–379.
14. Turcotte, R., Liang, Y., Tanimoto, M., et al. (2019). Dynamic super-resolution structured illumination imaging in the living brain. Proc. Natl. Acad. Sci. USA ***116***, 9586–9591.
15. Lin, R., Kipreos, E.T., Zhu, J., et al. (2021). Subcellular three-dimensional imaging deep through multicellular thick samples by structured illumination microscopy and adaptive optics. Nat. Commun. ***12***, 3148.
16. Zhao, W., Zhao, S., Li, L., et al. (2022). Sparse deconvolution improves the resolution of live-cell super-resolution fluorescence microscopy. Nat. Biotechnol. ***40***, 606–617.
17. Sahl, S.J., Balzarotti, F., Keller-Findeisen, J., et al. (2016). Comment on "Extended-resolution structured illumination imaging of endocytic and cytoskeletal dynamics". Science ***352***, 527–a.
18. Gustafsson, M.G. (2000). Surpassing the lateral resolution limit by a factor of two using structured illumination microscopy. J. Microsc. ***198***, 82–87.
19. Heintzmann, R., and Cremer, C.G. (1999). Laterally Modulated Excitation Microscopy: Improvement of Resolution by Using a Diffraction Grating. Optical Biopsies and Microscopic Techniques III (Proceedings of SPIE).
20. Křížek, P., Lukeš, T., Ovesný, M., et al. (2016). SIMToolbox: a MATLAB toolbox for structured illumination fluorescence microscopy. Bioinformatics ***32***, 318–320.
21. Müller, M., Mönkemöller, V., Hennig, S., et al. (2016). Open-source image reconstruction of super-resolution structured illumination microscopy data in ImageJ. Nat. Commun. ***7***, 1–6.
22. Lal, A., Shan, C., and Xi, P. (2016). Structured illumination microscopy image reconstruction algorithm. IEEE J. Sel. Top. Quantum Electron. ***22***, 50–63.
23. Wen, G., Li, S., Wang, L., et al. (2021). High-fidelity structured illumination microscopy by point-spread-function engineering. Light Sci. Appl. ***10***, 1–12.
24. Demmerle, J., Innocent, C., North, A.J., et al. (2017). Strategic and practical guidelines for successful structured illumination microscopy. Nat. Protoc. ***12***, 988–1010.
25. Fan, J., Huang, X., Li, L., et al. (2019). A protocol for structured illumination microscopy with minimal reconstruction artifacts. Biophys. Rep. ***5***, 80–90.

26. Karras, C., Smedh, M., Förster, R., et al. (2019). Successful optimization of reconstruction parameters in structured illumination microscopy–a practical guide. Opt Commun. ***436***, 69–75.
27. Chu, K., McMillan, P.J., Smith, Z.J., et al. (2014). Image reconstruction for structured-illumination microscopy with low signal level. Opt Express ***22***, 8687–8702.
28. Markwirth, A., Lachetta, M., Mönkemöller, V., et al. (2019). Video-rate multi-color structured illumination microscopy with simultaneous real-time reconstruction. Nat. Commun. ***10***, 1–11.
29. Wang, Z., Zhao, T., Hao, H., et al. (2022). High-speed image reconstruction for optically sectioned, super-resolution structured illumination microscopy. Adv. Photonics ***4***, 026003.
30. Perez, V., Chang, B.J., and Stelzer, E.H.K. (2016). Optimal 2D-SIM reconstruction by two filtering steps with Richardson-Lucy deconvolution. Sci. Rep. ***6***, 37149.
31. Richardson, W.H. (1972). Bayesian-based iterative method of image restoration. J. Opt. Soc. Am. ***62***, 55–59.
32. Lucy, L.B. (1974). An iterative technique for the rectification of observed distributions. Astron. J. ***79***, 745.
33. Sibarita, J.-B. (2005). Deconvolution microscopy. In Microscopy Techniques, J. Rietdorf, ed. (Springer Berlin Heidelberg), pp. 201–243.
34. O'Holleran, K., and Shaw, M. (2014). Optimized approaches for optical sectioning and resolution enhancement in 2D structured illumination microscopy. Biomed. Opt Express ***5***, 2580–2590.
35. Zhanghao, K., Chen, X., Liu, W., et al. (2019). Super-resolution imaging of fluorescent dipoles via polarized structured illumination microscopy. Nat. Commun. ***10***, 4694.
36. Qian, J., Cao, Y., Bi, Y., et al. (2023). Structured illumination microscopy based on principal component analysis. eLight ***3***, 4.
37. Qiao, C., Li, D., Guo, Y., et al. (2021). Evaluation and development of deep neural networks for image super-resolution in optical microscopy. Nat. Methods ***18***, 194–202.
38. Orieux, F., Sepulveda, E., Loriette, V., et al. (2012). Bayesian estimation for optimized structured illumination microscopy. IEEE Trans. Image Process. ***21***, 601–614.
39. Dong, S., Liao, J., Guo, K., et al. (2015). Resolution doubling with a reduced number of image acquisitions. Biomed. Opt Express ***6***, 2946–2952.
40. Ströhl, F., and Kaminski, C.F. (2017). Speed limits of structured illumination microscopy. Opt. Lett. ***42***, 2511–2514.
41. Gordon, G.W., Berry, G., Liang, X.H., et al. (1998). Quantitative fluorescence resonance energy transfer measurements using fluorescence microscopy. Biophys. J. ***74***, 2702–2713.
42. Du, M., Yang, F., Mai, Z., et al. (2018). FRET two-hybrid assay by linearly fitting FRET efficiency to concentration ratio between acceptor and donor. Appl. Phys. Lett. ***112***, 153702.

ACKNOWLEDGMENTS

This work was supported by the National Key Research and Development Program of China (2022YFF0712500), the Natural Science Foundation of China (NSFC) (62135003, 62005208, 62205267, 12204380), the Innovation Capability Support Program of Shaanxi (program no. 2021TD-57), and the Natural Science Basic Research Program of Shaanxi (2022JZ-34, 2020JQ-072, 2022JQ-069); NIH grants GM144414 to P.R.B.; and a Preliminary Data and Application Preparation Grant to P.R.B. and K.W. We appreciate Standard Imaging (Beijing) Biotechnology Co. Ltd for assistance with sample preparation.

AUTHOR CONTRIBUTIONS

Z.W., T.Z., and M.L. planned the study and drafted the manuscript. Z.W. and T.Z. contributed to data analysis and interpretation. H.H., P.R.B., and K.O. performed the sample preparation. Y.C., J.Z., Y.L., S.W., Y.S., and T.C. participated in manuscript revision. All authors have given final approval for the manuscript to be published and have agreed to be responsible for all aspects of the manuscript.

DECLARATION OF INTERESTS

Z.W. and M.L. are applying for a patent on JSFR-AR-SIM method. All other authors declare no competing interests.

SUPPLEMENTAL INFORMATION

It can be found online at https://doi.org/10.1016/j.xinn.2023.100425.

LEAD CONTACT WEBSITE

Ming Lei, http://www.opticaltweezers.net/